

Thermal Performance of Type III and IV Hydrogen Tanks Under Passive and Active Cooling[#]

Antar M. M. Abdala¹, Andrea Luigi Facci^{1*}, Marco Maggini¹, Misbah Aslam¹, Stefano Ubertini¹

¹ Department of Economics, Engineering, Society and Business Organization, University of Tuscia, 01100 Viterbo, Italy

(Corresponding Author: andrea.facci@unitus.it)

ABSTRACT

This study investigates the feasibility of cooling on-board hydrogen storage tanks using passive (fins) and active (forced water convection) methods. Two tank types (III and IV), two target pressures (35 and 70 MPa), and two chilled temperatures (-40°C and -20°C) are analyzed. Results show that Type IV tanks, especially under 70 MPa and 35 MPa, benefit most from cooling. Forced water convection significantly reduces hydrogen gas, liner, and shell temperatures, as well as heat transfer rates, compared to free convection.

Validation against previous studies confirms good agreement, and findings indicate that cooling (particularly forced convection) effectively limits peak temperatures and enhances refueling performance.

Under 70 MPa, -40°C, and Type IV tank conditions, forced convection at a water flow rate of 1 kg/s reduces the maximum temperatures of hydrogen, the liner, and the shell by 1.6 °C, 6 °C, and 13 °C, respectively, compared to free convection. In contrast, under 70 MPa, -20°C, and Type IV conditions, the corresponding reductions in maximum temperatures are 16 °C for hydrogen, 23 °C for the liner, and 32 °C for the shell walls.

Keywords: green hydrogen, hydrogen station, on-board hydrogen tank, cooling techniques

NONMENCLATURE

Abbreviations	
APRR	Average pressure ramp rate
FCEV	Fuel cell electric vehicle
H70, H35	Pressure class for a hydrogen fueling protocol with a NWP of 70 MPa, 35 MPa
HRS	Hydrogen refueling station
HP	High pressure
LP	Low pressure
MP	Medium pressure

NU	Nusselt Number
NWP	Nominal Working Pressure
TT	Tube trailer
T40, T20	Fuel delivery temperature category (-40°C, -20°C)
<i>Symbols</i>	
\dot{m}	Mass flow rate [kg/s]
h	Enthalpy [J/kgK]
u	Internal energy [J/kgK]

1. INTRODUCTION

Rapid refueling of compressed hydrogen storage systems (CHSS) for light- and heavy-duty vehicles is central to hydrogen mobility. The industry standard fueling protocols (most notably SAE J2601 and its heavy-duty variants) specify fueling trajectories, target pressures and nozzle supply temperatures (e.g., T40 \approx -40 °C precooling options) intended to keep tank/liner temperatures and structural stresses within permissible limits while achieving customer-target refueling times [1].

In the present study, cooling on board hydrogen tank will be investigated with different methods. A thermodynamic and heat transfer analysis is required to investigate the transient behavior of flow and heat transfer within the hydrogen tank.

Literature on refueling models spans a spectrum from computationally cheap lumped (0-D) models to full three-dimensional (3-D) conjugate heat transfer (CHT) computational fluid dynamics (CFD) simulations. Each class of model serves different use cases and faces distinct validation challenges. Zero-dimensional (lumped) thermodynamic models treat the tank interior as one or a few control volumes and solve transient mass and energy balances to obtain overall pressure and mean gas temperature trajectories. They are computationally inexpensive but cannot capture local hotspots [2].

[#] This is a paper for the 17th International Conference on Applied Energy (ICAE2025), December 8-12, 2025, Bangkok, Thailand.

1-D / 2-D axisymmetric transient models couple the gas energy equation with transient heat conduction in the tank wall and liner. They provide better prediction of wall temperatures and stratification than 0-D models [3-5].

CFD with conjugate heat transfer (CHT) solves the full Navier–Stokes and energy equations for the gas and solid tank layers. It resolves nozzle jets, turbulent mixing, and local hotspots but is computationally expensive [6].

System-level models integrate tank thermodynamics with station components such as compressors, cascade banks, and pre-coolers. They are critical for evaluating cascaded fills and station throughput [7-8]. This review identifies the need for a safe method to cool the on-board hydrogen tank of fuel cell electric cars (FCEVs) to less than 85°C.

So, in this current study, cooling methods for on-board hydrogen tanks are used for distinct tank types (III and IV), chilled temperatures (-40°C and -20°C), and target pressures (70 MPa and 35 MPa). The temperatures of the hydrogen, liner, and shell, as well as the energy transfer through the tank, will be evaluated under these conditions.

2. METHODOLOGY

2.1 Problem statement

In this study, we assess the impact of the on-board hydrogen storage cooling on the performance of a hydrogen refueling station (HRS). The HRS setup consists of a hydrogen source (tube trailer (TT) at 20 MPa) and a cascade storage system with low-, medium-, and high-pressure tanks. Additional components include filters, a pressure reduction valve, a mass flow meter, a chiller unit, and a dispenser. The on-board storage tank of a fuel cell electric vehicle (FCEV) is refueled using this HRS, as illustrated in Fig. 1.

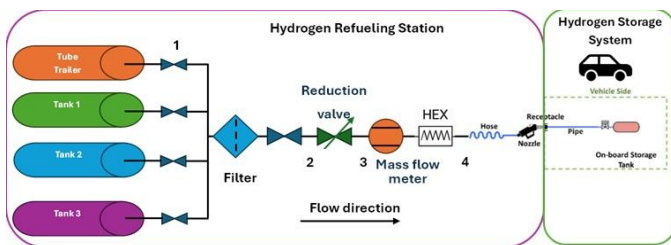


Fig. 1. HRS under test.

The specifications of HRS parameters are shown in Tab. 1.

This work investigates cooling of the on-board hydrogen tank to reduce the temperature of the incoming hot gas as well as the liner and shell wall temperatures.

Table 1. HRS parameters.

Parameters	Value
TT. pressure / volume	20 MPa/ 5 m ³
LP/ volume	33 MPa/1 m ³
MP/ volume	55 MPa/ 1 m ³
HP/ volume	90 MPa/ 1 m ³
Chiller Temperature	-40°C/-20°C
Target pressure	70MPa/35MPa

Two cooling methods are examined: (1) passive cooling using extended surfaces (fins) attached to the tank’s outer wall, and (2) active cooling via forced water convection through a serpentine tube with a rectangular cross-section. Simulations are carried out in MATLAB and validated against results from previous studies.

The on-board hydrogen tank parameters are based on the data provided in [5]. In contrast, this study considers a time-varying hydrogen mass flow rate rather than a constant one.

In this work, two FCEVs are analyzed, as summarized in Tab. 2. The tests are conducted at T40 (-40°C) and T20 (-20°C), keeping the APRR at the T40 level, to assess fast charging performance under reduced cooling demands of the HRS.

Table 2. Operating conditions.

Tank type	Target pressure	Chilled Temperature/APRR
IV	70MPa	T40 (18.5MPa/min)
IV	70MPa	T20 (5.5MPa/min)
IV	70MPa	T20 with the same APRR of T40 (18.5MPa/min)
IV	35 MPa	T40 (18.5MPa/min)
IV	35 MPa	T40 (5.5MPa/min)
IV	35 MPa	T20 (5.5MPa/min)
IV	35 MPa	T20 with the same APRR of T40 (18.5MPa/min)

III	35 MPa	T40 (18.5MPa/min)
III	35 MPa	T20 (5.5MPa/min)
III	35 MPa	T20 with the same APRR of T40 (18.5MPa/min)

Fin thickness	0.001 [m]
Number of fins	400
Thermal conductivity (Al)	238 [W/mK]
Total height	1.4 [m]

From J2601 standard, the values of operating conditions are show in Tab. 3 and Tab. 4.

Table 3. Operating conditions of- H35 [1].

Ambient Temp. [°C]	APRR [MPa/min]	Initial Tank Pressure, [MPa]	Target Pressure, [MPa]
25	18.5	2	38.2 (T40)
25	5.5	2	37.4 (T20)

Table 4. Operating conditions of - H70 [1].

Ambient Temp. [°C]	APRR [MPa/min]	Initial Tank Pressure, [MPa]	Target Pressure, [MPa]
25	18.5	2	72.8 (T40)
25	5.5	2	72.8 (T20)

2.1.1 Scenario 1: Annular fin cooling method

In this method, annular fins are mounted around the hydrogen tank, as illustrated in Fig. 2, with their specifications summarized in Tab. 3.

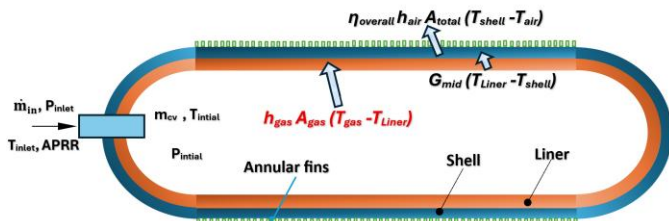


Fig. 2. Tank with passive cooling.

Table 3 Annular fin parameters

fin length	0.003 [m]
------------	-----------

2.1.2 Scenario 2: Forced convection cooling technique

With this method, a serpentine tube with a rectangular cross-section of 10 mm × 100 mm is arranged around the hydrogen tank, as shown in Fig. 3. The serpentine has a total length of 1.4 m. During the hydrogen charging process of fuel cell electric vehicles, the radiator coolant (water) flows through the rectangular duct. Coolant mass flow rates of 0.1 kg/s, 0.5 kg/s, and 1 kg/s are considered. The radiator already mounted on the vehicle has a heat rejection capacity of 36 kW at a coolant flow rate of 100 L/min (1.7 kg/s) [9].

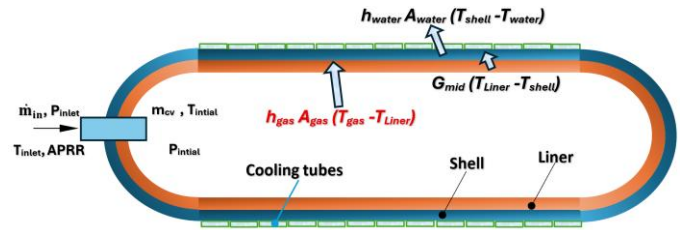


Fig. 3. Tank with active cooling.

2.2 The governing equations

The continuity and energy equations are applied to the on-board hydrogen tank control volume (CV) [5,8], assuming that $\dot{m}_{out} = 0$ and $\dot{W} = 0$:

$$\frac{dm_{cv}}{dt} = \dot{m}_{in} \quad (1)$$

$$\frac{d(m_{cv} * u_{cv})}{dt} = \dot{Q} + \dot{m}_{in} * h_{in} \quad (2)$$

Thus, the final expression for the internal energy of the hydrogen gas inside the tank is given as follows:

$$\frac{du_{cv}}{dt} = \frac{\dot{m}_{in}}{m_{cv}} * (h_{in} - u_{cv}) - \frac{\dot{Q}_{gas-Liner}}{m_{cv}} \quad (3)$$

In this study, CoolProp library [10] is employed to obtain the thermophysical properties of hydrogen. The heat transfer rate from the hot gas to the liner is then

calculated using Newton's law of cooling, as expressed below:

$$\dot{Q}_{gas-Liner} = h_{gas} * A_{gas} * (T_{gas} - T_{Liner}). \quad (4)$$

The hydrogen mass flow rate is determined using the pressure drop equation, expressed as follows:

$$P_{inlet} = P_{intial_{CV}} + APRR * time, \quad (4)$$

$$\Delta P = P_{inlet} - P_{cv}, \quad (5)$$

$$\Delta P = 0.5 * Kp * \rho * \dot{V}^2, \quad (6)$$

$$\dot{V} = \sqrt{\frac{2 * \Delta P}{Kp * \rho}}, \quad (7)$$

$$\dot{m}_{in} = \rho * \dot{V}. \quad (8)$$

Here, $Kp = 0.35$ [8]. A heat transfer balance is applied across the liner and shell materials to determine the temperatures of the liner and shell walls, as well as the corresponding heat transfer rates through these walls [5]:

$$\frac{d(m_{Liner} * C_{Liner} * T_{Liner})}{dt} = \dot{Q}_{gas-Liner} - \dot{Q}_{Liner-Shell}, \quad (9)$$

$$\dot{Q}_{Liner-Shell} = A_{mid} a_{mid} * (T_{Liner} - T_{Shell}), \quad (10)$$

$$\frac{d(m_{shell} * C_{shell} * T_{shell})}{dt} = \dot{Q}_{Liner-Shell} - \dot{Q}_{shell-ambient}. \quad (11)$$

For free convection, the heat transfer rate is:

$$\dot{Q}_{shell-ambient} = h_{air} * A_{shell\ outer} * (T_{shell} - T_{air}). \quad (12)$$

For extended surfaces, the heat transfer rate is:

$$\dot{Q}_{shell-ambient} = h_{air} * A_{total} * \eta_{overall} * (T_{shell} - T_{air}). \quad (13)$$

For forced convection, the heat transfer rate is:

$$\dot{Q}_{shell-ambient} = h_{forced} * A_{design} * (T_{shell} - T_{avg\ water}). \quad (14)$$

The helical diameter D_c and Dean number De are calculated as follows:

$$D_c = (2 * r_o) + D_h, \quad (15)$$

$$De = Re \sqrt{\frac{D_h}{D_c}}. \quad (16)$$

For $Re < 2300$, the Nusselt number correlation for helical pipes proposed by Liu and Masliyah [11] is used. The valid ranges for this correlation are $20 < De < 5000$ and $0.1 < Pr < 500$.

$$\begin{aligned} Nu &= 3.657 \\ &+ \frac{(0.75 De^{1/2} + 0.0028Pr)Pr^{1/8}}{(1 + 0.00174 Pr^{-3})(1 + 70.6 \frac{Pr^{-0.6}}{De})} \end{aligned} \quad (17)$$

For turbulent flow, the Nusselt number correlation of Gnielinski (1986) [12] is used. The valid ranges for this correlation are $2.2 \times 10^4 < Re$, and $0.714 < Pr < 6.0$.

$$f = \frac{0.3164}{Re^{0.25}} + 0.03 \sqrt{\frac{D_h}{D_c}}, \quad (18)$$

$$Nu = \frac{\frac{f}{8} * Re * Pr}{(1 + 12.7 * \sqrt{\frac{f}{8}} * (Pr^{\frac{2}{3}} - 1))}. \quad (19)$$

Where f is the friction factor. We get the overall fin efficiency $\eta_{overall}$ as follows, taking into account the fin geometry as shown in Fig.4 [13]:

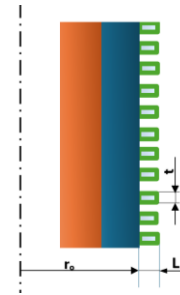


Fig. 4. Liner and shell with fins.

Calculate m parameter as follows:

$$m = \sqrt{\left(\frac{2 * h_{air}}{(k * th)}\right)}, \quad (20)$$

The fin efficiency is calculated as follows:

$$\eta_f = C_2 \frac{K_1(mr_1)I_1(mr_{2c}) - I_1(mr_1)K_1(mr_{2c})}{I_0(mr_1)K_1(mr_{2c}) + K_0(mr_1)I_1(mr_{2c})}, \quad (21)$$

$$C_2 = \frac{2r_1/m}{\{m(r_{2c}^2 - r_1^2)\}} \quad (22)$$

Surface area calculation as below:

$$A_f = 2 * \pi * (r_{2c}^2 - r_1^2). \quad (23)$$

We calculate the corrected outer radius as below:

$$r_{2c} = r_2 + \frac{th}{2} \quad (24)$$

The total surface area is calculated as follows:

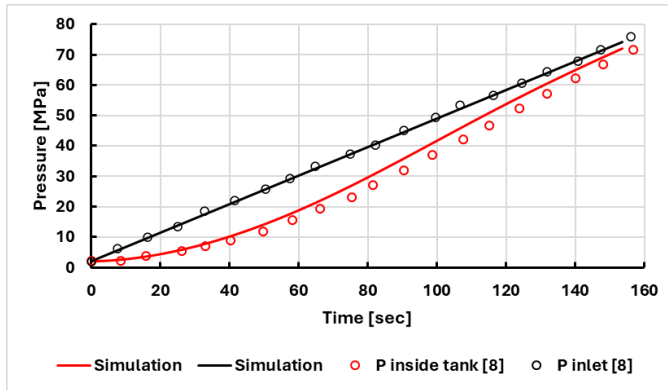
$$A_{tot} = \pi * 2 * r_o * (L_{design} - (N_f * th)) + (N_f * A_f) \quad (25)$$

Finally, the overall fin efficiency is calculated as follows:

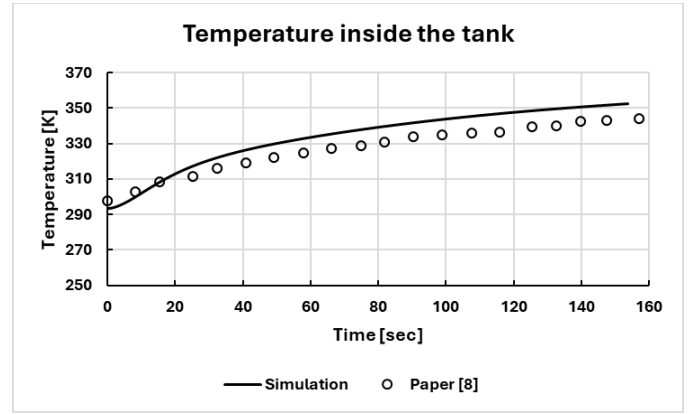
$$\eta_{overall} = 1 - \left(\frac{N_f * A_f * 1 - \eta_f}{A_{tot}} \right) \quad (26)$$

2.3 Validation for simulation

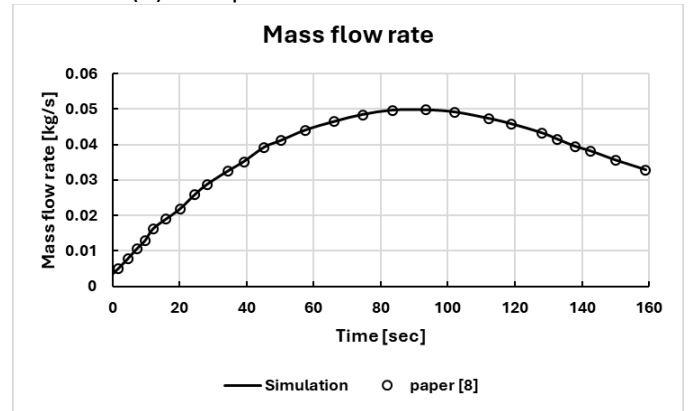
In this study, the HRS simulation is validated against previous work [8]. For this validation, the buffer tank at 90 MPa and the cascade system are compared with the results from [8]. The parameters used for validation include pressure, temperature, mass flow rate, and cooling demand.



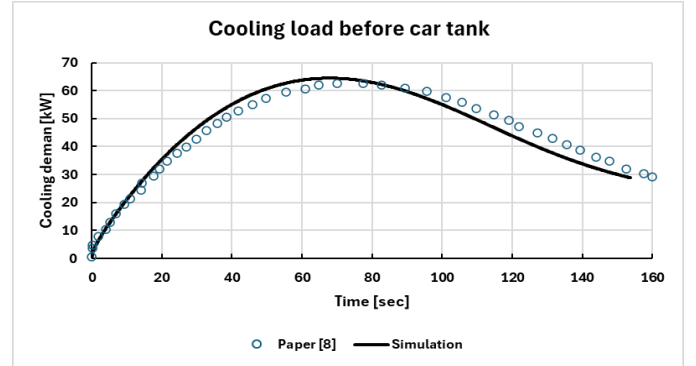
(a) Inlet pressure and inside pressure of tank



(b) Temperature inside the tank



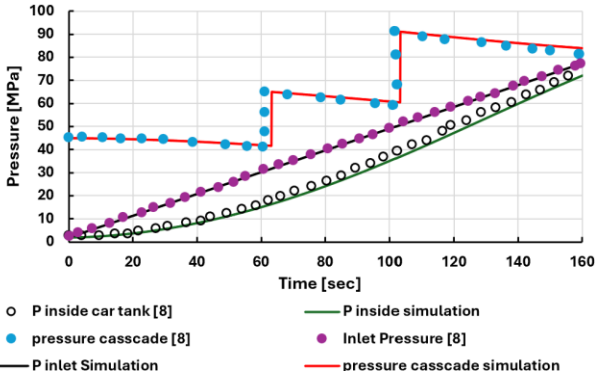
(c) Hydrogen mass flow rate



(d) Cooling demand of chiller unit

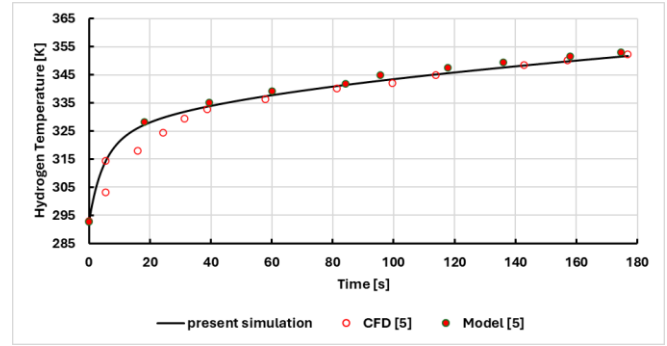
Fig. 5. Comparison between previous work [8] and simulation results for a high-pressure buffer tank: (a) pressure, (b) temperature, (c) mass flow rate, and (d) cooling demand.

The validation of the cascade system is presented in the following figures.

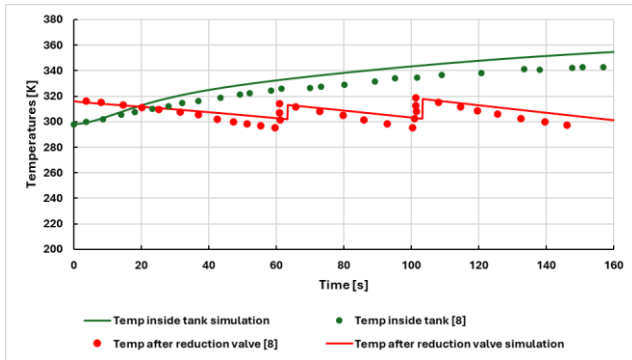


(a) Inlet pressure and inside pressure of on-board tank and pressure inside cascade tanks

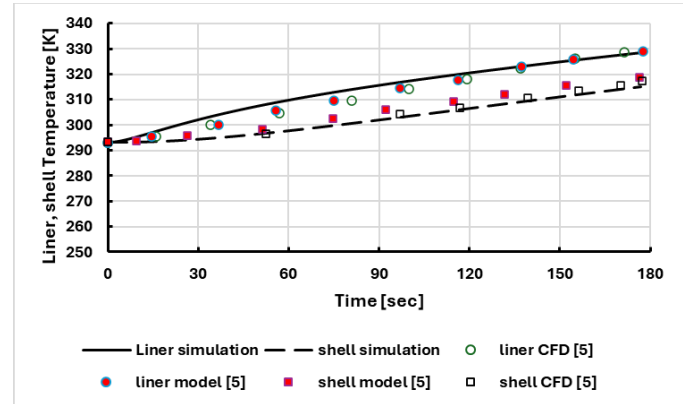
To validate the liner and shell temperatures, an additional comparison is performed against the results reported in [5].



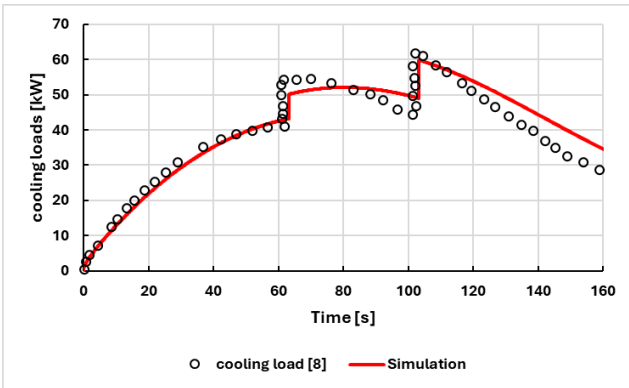
(a) Hydrogen gas temperature of tank type III



(b) temperature inside on-board tank and temperature after reduction valve



(b) Liner and shell temperatures of tank type III



(c) Cooling demand of chiller unit

Fig. 7. validation between other work [5] and simulation: (a) hydrogen Temperatures, and (b) liner and shell temperatures

3. RESULTS AND DISCUSSION

3.1 H70-T40 IV Cooling

Fig. 8 illustrates the variation of hydrogen gas temperature inside the on-board tank over time during charging, using free convection, fins, and forced convection cooling techniques. It is evident that the hydrogen temperature drops more rapidly after 120 s under forced convection with a high water flow rate. The maximum hydrogen temperature decreases by 1.7 °C with forced convection at 1 kg/s compared to free convection.

Fig. 6. validation between other work [8] and simulation for cascade tanks: (a) pressure, (b) temperature, and (c) cooling demand.

As shown in Fig. 5 and Fig. 6, the simulation results exhibit good agreement with the findings of previous work [8].

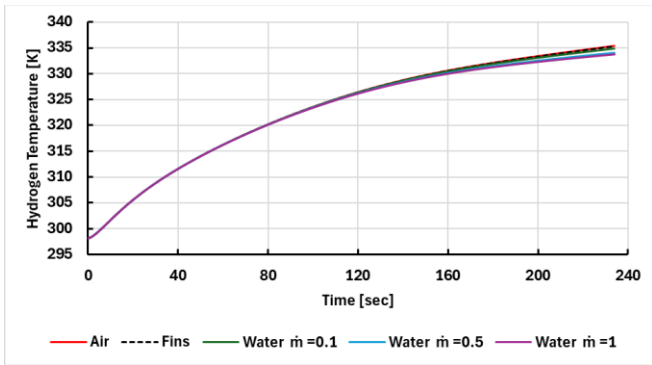


Fig. 8. Hydrogen temperature inside cooled on-board tank with different methods

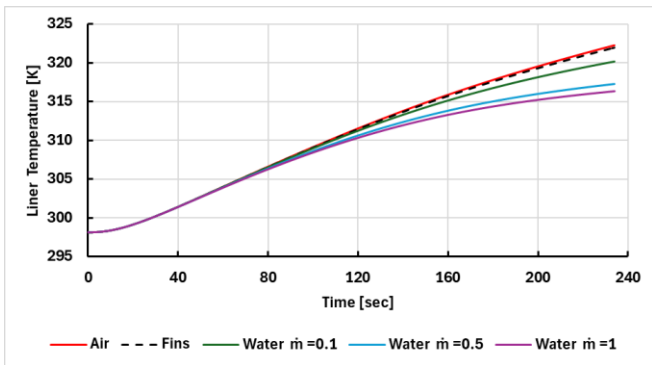


Fig. 9. Liner temperature of cooled on-board tank with different methods

Fig. 9 shows the time variation of the tank's composite liner temperature under different cooling techniques. The maximum liner temperature decreases by approximately 6 °C with forced convection at a high flow rate compared to free convection.

Fig. 10 illustrates the corresponding shell temperature over time for the cooled tank. Using forced convection at a high flow rate reduces the maximum shell temperature by 13 °C relative to free convection.

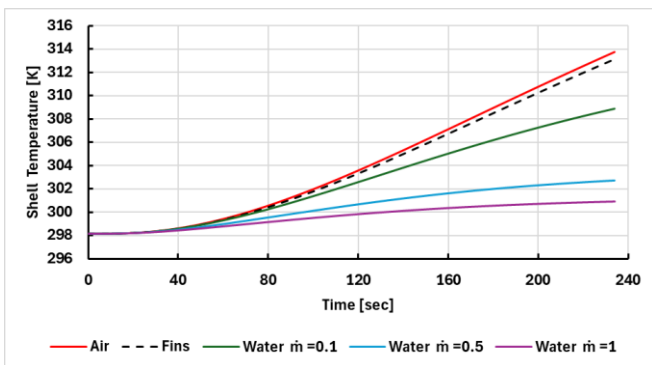


Fig. 10. Shell temperature of cooled on-board tank with different methods

Fig. 11 shows the heat transfer rate from the hot hydrogen gas to the tank's liner wall under different cooling techniques. It is evident that the heat transfer rate increases with water forced convection, reaching 1.3 times higher rates at the higher water flow rate compared to free convection.

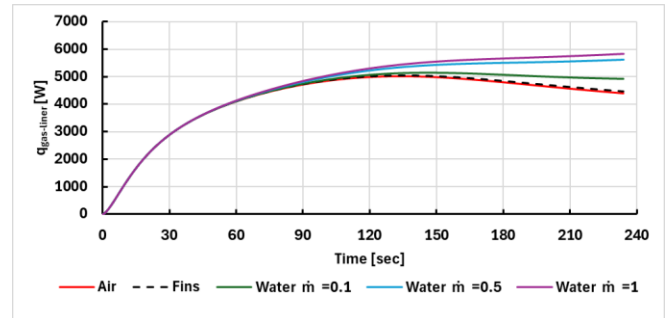


Fig. 11. Heat transfer rate from hot gas to liner wall of cooled on-board tank with different methods

Fig. 12 illustrates the variation of heat transfer rate from the tank's shell wall to the ambient under different cooling methods. It is evident that air free convection cannot remove the large amount of heat stored in the tank walls. In contrast, forced convection at a high water flow rate extracts approximately 25 times more heat than free convection.

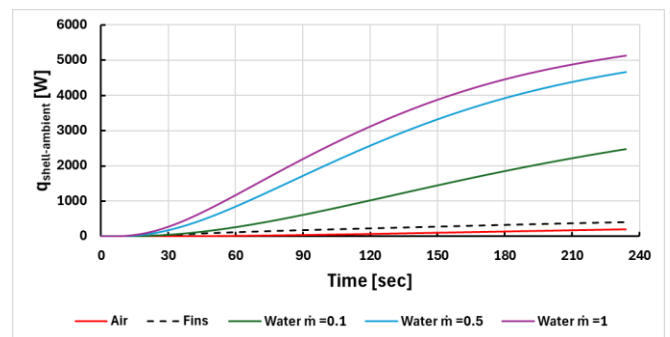
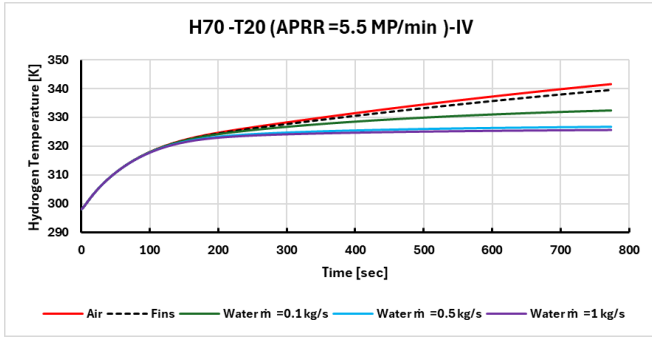


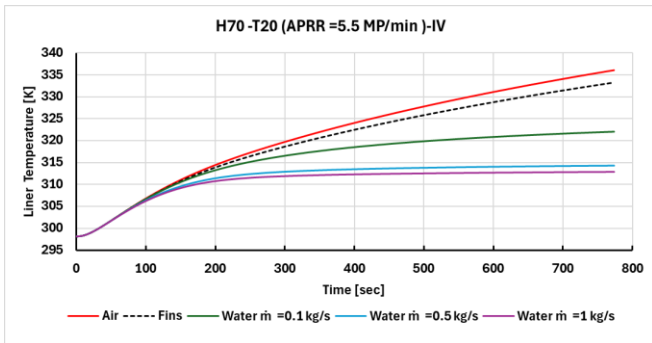
Fig. 12. Heat transfer rate from shell wall to ambient using different cooling conditions

3.2 H70-T20 IV Cooling

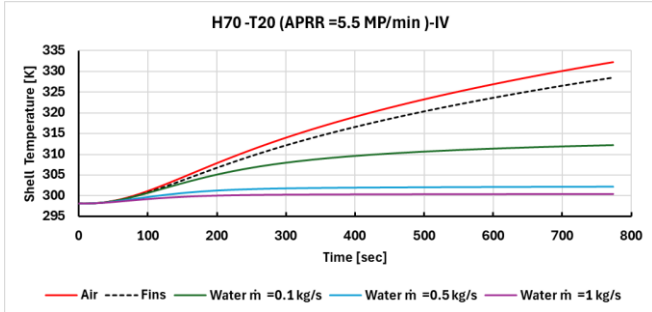
Fig. 13 illustrates the time-dependent variation of hydrogen, liner, and shell temperatures at H70 and T20, where the APRR is 5.5 MPa/min.



a. Hydrogen Temperature



b. Liner Temperature



c. Shell Temperature

Fig. 13. Temperatures at H70-T20: (a)Hydrogen, (b)liner, and (C) shell temperatures .

It is evident that applying cooling reduces temperatures, particularly at higher chilled temperatures. With forced convection at a high water flow rate, the maximum temperatures of the hydrogen gas, liner, and shell walls decrease by 16 °C, 23 °C, and 32 °C, respectively, compared to free convection.

Furthermore, cooling is more effective under H70–T20 conditions than under H70–T40 (see Fig. 8 and Fig. 10).

3.3 H70-T20 IV with APRR of T40 Cooling

In this method, the chilled temperature is increased to –20 °C instead of –40 °C while maintaining the same APRR. The APRR is 18.5 MPa/min at T40 (faster charging) compared with 5.5 MPa/min at T20 (slower charging).

The goal is to enable fast charging, reduce the cooling demand of the HRS, and lower the hydrogen gas and tank wall temperatures. Fig. 14 presents the maximum hydrogen, liner, and shell temperatures under the different cooling techniques.

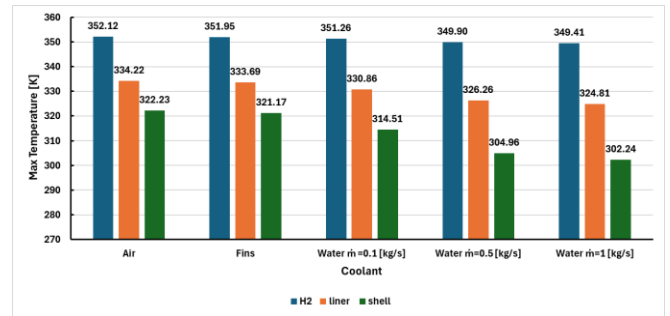
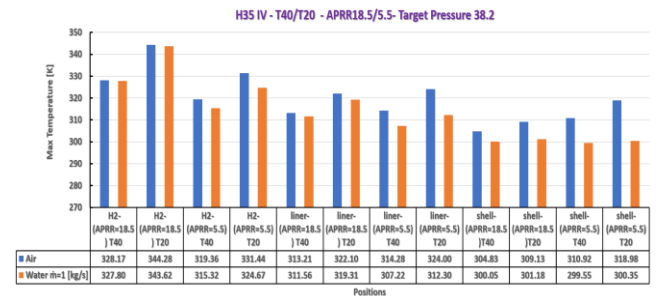


Fig. 14. Max hydrogen, liner, and shell temperatures at high chilled temperature with fasting charging.

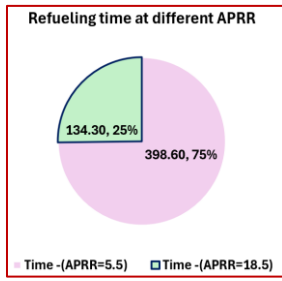
It is evident that forced water convection at a high flow rate reduces the maximum hydrogen, liner, and shell temperatures by approximately 3 °C, 19 °C, and 20 °C, respectively, compared to free convection.

3.4 H35-T40 IV and T20 with APRR of T40 Cooling

Fig. 15 compares the maximum hydrogen, liner, and shell temperatures at T40 and T20, at APRR of 18.5 and 5.5 MPa/min, for a target pressure of 35 MPa and a Type IV tank.



(a)



(b)

Fig. 15. (a) Max hydrogen, liner, and shell temperatures at H35-IV-T40 and T20 with APRR =18.5 and 5.5 MPa/minute. (b) refueling time at different APRR

It is evident that the cooling effect on maximum temperatures is less pronounced at T40 compared to T20 under the same APRR. This indicates that a higher chilled temperature (-20 °C) can be effectively used for tank cooling without compromising safety.

At high APRR, water cooling enables much faster refueling with a moderate temperature rise, still within Type IV tank safety limits. Increasing the coolant temperature from -40 °C to -20 °C slightly raises in-tank temperatures but significantly reduces cooling demand. Overall, water cooling demonstrates better performance than air cooling across conditions.

3.5 H35- III- T40 and T20 at APRR of 18.5 MPa/min

Fig. 16 shows the maximum temperature values for a Type III tank at different chilled temperatures with the same APRR of 18.5 MPa/minutes.

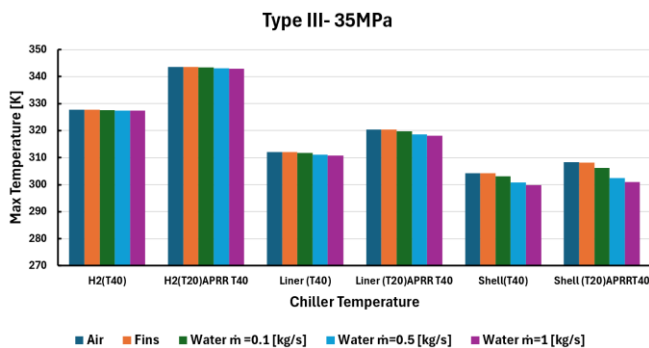


Fig. 16. Max hydrogen, liner, and shell temperatures at H35-III-T40 and T20 with same APRR of 18.5 MPa/min.

At a target pressure of 35 MPa, the cooling effect is less significant for the Type III tank under the lower chilled temperature (T40). In contrast, water cooling at

the higher chilled temperature (T20) proves more effective, especially in reducing liner and shell temperatures. For both H35-T40 III and H35-T20 III at APRR = 18.5, the refueling time remains the same, while temperatures increase slightly but stay below the safety limit of 85 °C (358 K).

3.6 H35-T20 III and with APRR of 18.5 and 5.5 MPa/min

Fig. 17 shows the maximum temperature values for a Type III tank at different chilled temperatures with the same APRR of 18.5 MPa/minutes. The results indicate that for a Type III tank filled to 35 MPa, cooling has a minor effect at high APRR, while at low APRR, its influence becomes much more significant. For the H35-T20 III condition, increasing the APRR from 5.5 to 18.5 reduces the refueling time from 390 s to 132 s, with all temperatures remaining safely below the 85 °C (358 K) limit.

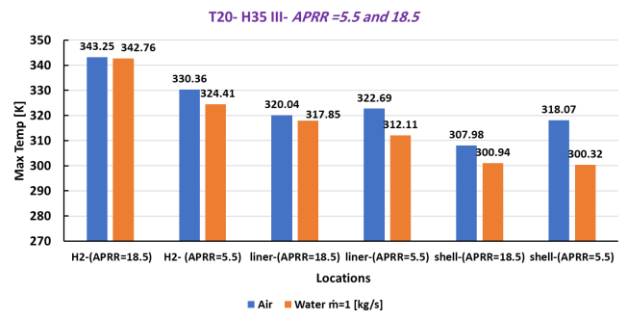


Fig. 17. Max hydrogen, liner, and shell temperatures at H35-T20 III with APRR of 18.5 and 5.5 MPa/min.

4. CONCLUSIONS

This study examines the feasibility of cooling on-board hydrogen storage tanks using different techniques. Two cooling approaches are considered: passive cooling, represented by fins, and active cooling, represented by forced water convection around the tank.

The analysis is carried out for two tank types (Type III and Type IV), two target pressures (35 MPa and 70 MPa), and two chilled temperatures (-40°C and -20°C). The study investigates hydrogen gas, liner wall, and shell wall temperatures, as well as heat transfer rates from the hot gas into the liner and shell walls before being released to the surrounding environment. Simulation results are validated against previous studies, showing good agreement.

The findings highlight the importance of cooling Type IV tanks, particularly under 70 MPa and 35 MPa conditions, compared with Type III tanks at 35 MPa.

Among the tested methods, forced water convection proved most effective in reducing the temperatures of hydrogen gas, the liner, and shell walls, as well as decreasing heat transfer rates from the hot gas to the coolant. Free convection, by contrast, was less effective in extracting heat from the tank. The study also investigates the effect of increasing the HRS chilled temperature from -40°C to -20°C while using the APRR corresponding to -20°C . The results indicate that forced convection cooling is highly effective under these conditions, with maximum temperatures reduced by up to 93% compared to free convection.

The study further investigates the impact of increasing the HRS chilled temperature from -40°C to -20°C while keeping the average pressure ramp rate (APRR) fixed at -40°C , aiming to enable faster refueling at the higher chilled temperature (-20°C). The results show that cooling—especially via forced convection and in Type IV tanks—significantly reduces peak temperature values, enhancing thermal management during refueling. For the H70-T20 IV condition with an APRR equivalent to T40 cooling (18.5), the refueling time decreases sharply from 773.8 s to 234 s under high APRR. It is evident that forced water convection at a high flow rate effectively reduces the maximum hydrogen, liner, and shell temperatures by approximately 3°C , 19°C , and 20°C , respectively, compared to free convection.

The same effect of the cooling on a Type III and IV tank at a target pressure of 35 MPa across different chilled temperatures. At the higher chilled temperature (T20), water cooling is more effective than at the lower chilled temperature (T40).

ACKNOWLEDGEMENT

This project has been partially supported by the projects:

- PRIN P20223JMB3 - Modeling and optimization of sustainable hydrogen refueling infrastructures (HyREFI) and PRIN 2020BFX8JY - Hybrid Sustainable Mobility (HYSUM).

- ECS 0000024 Rome Technopole, CUP B83C22002820006, National Recovery and Resilience Plan (NRRP) Mission 4 Component 2 Investment 1.5, funded by the European Union-NextGenerationEU.

- National Recovery and Resilience Plan (NRRP), Mission 4 Component 2 Investment 1.3 - Call for tender No. 1561 of 11.10.2022 of Ministero dell'Università della

Ricerca (MUR); funded by the European Union-NextGenerationEU.

REFERENCES

- [1] SAE International. SAE J2601: Fueling Protocols for Light Duty Gaseous Hydrogen Surface Vehicles.
- [2] Daniele Melideo, Umberto Desideri, "Hydrogen tank filling simulation using a zero-dimensional model: Validation and effect of some key parameters", *International Journal of Hydrogen Energy*, Volume 72, 2024, <https://doi.org/10.1016/j.ijhydene.2024.05.444>
- [3] Dicken, C. J. B., & Mérida, W. (2007). Modeling the Transient Temperature Distribution within a Hydrogen Cylinder during Refueling. *Numerical Heat Transfer, Part A: Applications*, 53(7), 685–708. <https://doi.org/10.1080/10407780701634383>
- [4] Jinsheng Xiao, Xu Wang, Xin Zhou, Pierre Bénard, Richard Chahine, A dual zone thermodynamic model for refueling hydrogen vehicles, *International Journal of Hydrogen Energy*, Volume 44, Issue 17, <https://doi.org/10.1016/j.ijhydene.2018.10.235>.
- [5] Jinsheng Xiao, Nianfeng Xu, Wenchao Cai, Xin Zhou, Pierre Bénard, Richard Chahine, Liang Tong, Tianqi Yang, "Thermodynamic and heat transfer models for refueling hydrogen vehicles: Formulation, validation and application", *International Journal of Hydrogen Energy*, Volume 52, Part B, 2024, <https://doi.org/10.1016/j.ijhydene.2023.06.081>.
- [6] C. Hall, V. Ramasamy, "Modelling the conjugate heat transfer during the fast-filling of high-pressure hydrogen vessels for vehicular transport", *International Journal of Thermofluids*, Volume 21, 2024, <https://doi.org/10.1016/j.ijft.2023.100527>.
- [7] Hong, D.H., Kim, S.H., Karng, S.W. *et al.* Dynamic analysis of refueling characteristics of hydrogen refueling station. *J Mech Sci Technol* **38**, 4911–4920 (2024). <https://doi.org/10.1007/s12206-024-0826-1>
- [8] Rothuizen, E. D. (2013). *Hydrogen fuelling stations: A thermodynamic analysis of fuelling hydrogen vehicles for personal transportation* (PhD's thesis). Technical University of Denmark, Department of Mechanical Engineering.
- [9] Lee, H.-S.; Cho, C.-W.; Seo, J.-H.; Lee, M.-Y. "Cooling Performance Characteristics of the Stack Thermal Management System for Fuel Cell Electric Vehicles under Actual Driving Conditions". *Energies* **2016**, 9,320. <https://doi.org/10.3390/en9050320>
- [10] Ian H. Bell, Jorrit Wronski, Sylvain Quoilin, and Vincent Lemort, "Pure and Pseudo-pure Fluid Thermophysical Property Evaluation and the Open-Source Thermophysical

Property Library CoolProp," **Industrial & Engineering Chemistry Research**, 2014, 53(6), pp. 2498–2508.
<https://doi.org/10.1021/ie4033999>

- [11] Mehdi Ghobadi & Yuri Stephan Muzychka (2016) A Review of Heat Transfer and Pressure Drop Correlations for Laminar Flow in Curved Circular Ducts, *Heat Transfer Engineering*, 37:10, 815-839, DOI: 10.1080/01457632.2015.1089735.
<http://dx.doi.org/10.1080/01457632.2015.1089735>
- [12] Zhao, H., Li, X., Wu, Y., & Wu, X. (2020). Friction factor and Nusselt number correlations for forced convection in helical tubes. *International Journal of Heat and Mass Transfer*, 155, 119759. <https://doi.org/10.1016/j.ijheatmasstransfer.2020.119759>
- [13] Bergman, T. L., Lavine, A. S., Incropera, F. P., & DeWitt, D. P. (2017). *Fundamentals of heat and mass transfer* (8th ed.). Wiley.